Journal of Controlled Release 168 (2013) 18–27

Contents lists available at SciVerse ScienceDirect

Journal of Controlled Release

journal homepage: www.elsevier.com/locate/jconrel

Delivery of definable number of drug or growth factor loaded poly(DL-lactic acid-co-glycolic acid) microparticles within human embryonic stem cell derived aggregates

Omar Qutachi, Kevin M. Shakesheff, Lee D.K. Buttery *

Wolfson Centre for Stem Cells Tissue Engineering and Modelling, Centre of Biomolecular Sciences, School of Pharmacy, University of Nottingham, Nottingham, UK

ARTICLE INFO

Article history:
Received 10 December 2012
Accepted 24 February 2013
Available online 14 March 2013

Keywords:
Drug delivery
$P_{DL}LGA$
Microparticles
Simvastatin
Stem cells
Osteogenesis

ABSTRACT

Embryoid bodies (EBs) generated from embryonic stem cells are used to study processes of differentiation within a three dimensional (3D) cell environment. In many instances however, EBs are dispersed to single cell suspensions with a subsequent monolayer culture. Moreover, where the 3D integrity of an EB is maintained, cytokines or drugs of interest to stimulate differentiation are often added directly to the culture medium at fixed concentrations and effects are usually limited to the outer layers of the EB. The aim of this study was to create an EB model with localised drug and or growth factor delivery directly within the EB. Using poly(DL-lactic acid-co-glycolic acid) microparticles (MPs) with an average diameter of 13 μm, we have demonstrated controllable incorporation of defined numbers of MPs within human ES cell derived EBs, down to 1 MP per EB. This was achieved by coating MPs with human ES cell lysate and centrifugation of specific ratios of ES cells and MPs to form 3D aggregates. Using MPs loaded with simvastatin (pro or active drug) or BMP-2, we have demonstrated osteogenic differentiation within the 3D aggregates, maintained in culture for up to 21 days, and quantified by real time QPCR for *osteocalcin*. Immunostaining for RUNX2 and osteocalcin, and also histochemical staining with picrosirius red to demonstrate collage type 1 and Alizarin red to demonstrate calcium/mineralisation further demonstrated osteogenic differentiation and revealed regional staining associated with the locations of MPs within the aggregates. We also demonstrated endothelial differentiation within human ES cell-derived aggregates using VEGF loaded MPs. In conclusion, we demonstrate an effective and reliable approach for engineering stem aggregates with definable number of MPs within the 3D cellular structure. We also achieved localised osteogenic and endothelial differentiation associated with MPs releasing encapsulated drug molecules or cytokines directly within the cell aggregate. This provides a powerful tool for controlling and investigating differentiation within 3D cell cultures and has applications to drug delivery, drug discovery, stem cell biology, tissue engineering and regenerative medicine.

1. Introduction

In early development, morphogens are secreted locally to create a concentration gradient from a source to a sink, which diffuses over local groups of cells resulting in cells with different phenotypes [1–6]. In this context the location of a cell within this concentration gradient of the morphogen is an important determining factor for the lineage commitment towards a specific phenotype [4,7,8]. For *in vitro* studies, when comparing 2D and 3D models, cells often express more specific markers and demonstrate morphologies and characteristics that more closely resemble the native tissue when cultured in a 3D environment [9]. The orientation of cells within a 3D environment is also important in the determining of cell morphology, extracellular matrix (ECM) interactions, cell adhesion, differentiation and gene expression as well as protein level and functionality when compared to 2D monolayer culture [10–13]. Therefore, a 3D cell culture model can potentially provide a more reliable approach for applications in tissue engineering and regenerative medicine [14].

The multi-cellular aggregates or embryoid bodies (EBs) generated in the initial stages of differentiation of most embryonic stem cell lines provide a model that, to some extent, mimics the events during early development. This in turn can be useful for studying the effects of small molecules and/or biological agents [15,16] to induce and investigate differentiation [17–20]. However, in many instances after an initial period of cell aggregation, the resultant EBs are dissociated to single cell suspensions with subsequent culture of the dispersed cells as monolayers [21,22]. Other studies have preserved the 3D EB structure by plating of the whole EBs [23–25].

In addition to methods for controlling cell–cell interactions, growth factors and drugs are often required to help stimulate differentiation and typically these are added directly to the culture medium at fixed

* Corresponding author at: School of Pharmacy, Centre for Biomolecular Sciences, University of Nottingham, Nottingham, NG7 2RD, UK. Tel.: +44 115 846 7857; fax: +44 115 951 5121.
E-mail address: lee.buttery@nottingham.ac.uk (L.D.K. Buttery).

0168-3659/$ – see front matter © 2013 Elsevier B.V. All rights reserved.
http://dx.doi.org/10.1016/j.jconrel.2013.02.029

concentrations [24,26–28]. While this approach might work well for 2D monolayer cell culture, 3D culture models present challenges for delivery and uptake of growth factors and drugs and in many cases their effects are restricted to outer regions of the 3D model that is in direct contact with the culture medium. For drug delivery and tissue engineering purposes biodegradable polymer microparticles (MPs) should be capable, ideally, of presenting encapsulated molecules in a spatiotemporal way that suits the generation of the tissue of interest [29]. Poly(DL-lactic acid-co-glycolic acid) ($P_{DL}LGA$) co-polymers are widely used in tissue engineering and drug delivery. They are available in a range of molecular weights and lactide to glycolide ratio, which offers flexibility in controlling the degradation profile and release kinetics [30–32].

Recent work has demonstrated an improved and more homogeneous differentiation of cells within EBs using $P_{DL}LGA$ MPs loaded with retinoic acid in comparison to the traditional approach involving retinoic acid supplemented to the culture medium [33]. Although incorporation of MPs within EBs was successful, the process can be still variables in term of achieving a reproducible and comparable incorporation of a defined number of MPs among EBs. In this context, controlling release and delivery of growth factors within EBs using polymer MPs can result in an *in vitro* 3D model with a more reliable directed differentiation. This might also enable mimicking of morphogen gradients within the developing embryo [33,34].

The incorporation of $P_{DL}LGA$ MPs within EBs can be achieved by a simple mixing of ES cell–MPs suspensions [33,35]. However, poor cell attachment to the polymer surface due to polymer hydrophobicity is a major limitation [36–39]. The latter has been found to be improved by coating with materials like gelatin or agarose [40], collagen [41] cadherin [42] and poly-lysine [43]. Improving cell attachment to biomaterials can be also achieved either by adsorbing or conjugating ECM peptides or specific ECM–cell binding sequences on biomaterial surfaces [44–48] or using biotin–avidin cross-linking [49]. In recent years there has been an increasing interest in incorporating MPs within EBs with a focus on approaches to delivering MPs with and investigation of cellular compatibility and effects on germ layer differentiation and vasculogenesis [43–45,50,60].

A drawback with many of these studies is the limited control over the number of MPs incorporated within EBs, potentially resulting in variability in number of MPs per EB and affecting both amounts of the drug or cytokine delivered and subsequent cell responses. The incorporation of a defined number of MPs within the 3D multicellular structure of an EB can provide a model with a focal release of the molecule of interest from a localised area that can diffuse to the surroundings. This can provide an efficient differentiation model enhancing lineage commitment from a controlled number of MPs in comparison to the recent current model(s) using large numbers of MPs.

In this study we demonstrate an effective and efficient approach for incorporating definable numbers of $P_{DL}LGA$ MPs within human ES cell-derived aggregates. Using MPs loaded with simvastatin (pro and active drugs), bone morphogenetic protein 2 (BMP-2) or vascular endothelial growth factor (VEGF) we demonstrate localised osteogenic or endothelial differentiation within the aggregates. This provides a powerful tool for controlling and investigating differentiation within 3D cell cultures and has applications to drug delivery, drug discovery, stem cell biology, tissue engineering and regenerative medicine.

2. Materials and methods

2.1. Micro-particle fabrication

Microparticles (MPs) were fabricated from 14% $P_{DL}LGA$ 50:50 (52 kDa, Lakeshore Biomaterials, Inc., USA) in dichloromethane (DCM, Fisher, UK) by either single or double emulsion methods. In the single emulsion method, the polymer solution was homogenised in 250 ml of 0.3% polyvinyl alcohol (PVA, Sigma-Aldrich, UK) using a high speed homogeniser (Ultra-Turrax, T25 Basic IKA-Werke). The resulting emulsion was left stirring at 300 RPM until MPs hardened. In the double emulsion method, 50 μl of an aqueous solution containing the molecule of interest (VEGF or BMP-2) was homogenised in the polymer solution. The resultant primary water in oil (w/o) emulsion was then homogenised again in 0.3% PVA and the resultant water in oil in water (w/o/w) double emulsion was left stirring until MPs hardened.

Coumarin-6 [50,51] and/or CellTracker red [35] were used for labelling MPs and tracking their incorporation within EBs. Labelling was achieved during MP fabrication with 0.001% Coumarin-6 (Sigma-Aldrich, UK) and/or 0.02% CellTracker red (Invitrogen, UK).

Loading with simvastatin pro-drug (Calbiochem, UK) or simvastatin active drug (Calbiochem, UK) was done using a single emulsion. The statins were dissolved in the DCM with the polymer at 0.5% of the polymer weight. For the cytokines, 0.1% BMP-2, purchased from Professor Walter Sebald (University of Würzburg, Germany) or VEGF (PeproTech, UK) was encapsulated using the double emulsion method by dissolving 1 mg of the growth factor in 50 μl of 1% (w/v) human serum albumin and the process of MP fabrication was continued as described earlier. Extensive *in vitro* studies on the controlled release of drugs or cytokines encapsulated within these MPs have been performed in aqueous buffers over 3 weeks using 24 mm plates with 0.4 μm Transwell insert (Corning, UK). Aliquots of 100 mg of drug loaded PLGA MPs were suspended in PBS and incubated at 37 °C. The quantification of simvastatin was followed using Agilent 1090 high pressure liquid chromatography with UV detector (HPLC-UV). Isocratic separation was fulfilled with C18-Hypersil column (100 × 5 mm, i.d. 5 μm packing, Thermo Scientific, UK). The mobile phase included 15% of 1 mM ammonium acetate adjusted at pH 4.4 and 85% methanol. The flow rate was maintained at 1 ml per minute at 40 °C and detection was measured at 238 nm. BCA assay (Sigma-Aldrich, UK) for total protein was used for BMP-2 quantification and we have previously published on the use of a cell-based assay to measure the release of active BMP2 [52].

2.2. Micro-particle characterisation

The fabricated MPs were subjected to examination for surface morphology via scanning electron microscopy. In brief, MPs were loaded onto carbon discs (Agar Scientific, UK) mounted on aluminium stubs (Agar Scientific, UK). The MPs were gold-coated using a Balzers SCD 030 gold sputter coater (Balzers Union Ltd., Leichtenstein). Imaging of the MPs was done using a JEOL 6060L scanning electron microscope imaging system (JEOL Ltd., Hertfordshire, UK) at 10 kV ionising radiation. Mean diameter and particle size distribution were also investigated using a Coulter LS230 particle size analyser (Beckman, UK). The particle size distribution was then determined as a function of the particle diffraction and plotted as a function of volume percentage (Supplementary Fig. 1).

2.3. Embryoid body formation

Human embryonic stem cells (HUES-7) cultured under feeder free conditions were dissociated with 0.05% trypsin (Invitrogen, UK) and suspended in mouse embryonic fibroblast (MEF) cell conditioned medium consisting of DMEM-F12 (Gibco, UK) supplemented with 15% (v/v) Knockout serum (Gibco, UK), 1% L-glutamine (2 mM) and 0.01% 2-mercaptoethanol (100 μM) (Sigma-Aldrich, UK), 1% nonessential amino acids (Sigma-Aldrich, UK), and 8 ng/ml of FGF (Sigma-Aldrich, UK; 4 ng/ml was supplemented before the medium conditioning with MEF cells and another 4 ng/ml supplemented before use). Cell suspensions at 1×10^6 cell/ml were transferred to 96 multi-well plate with V-shaped bottom (Sero-Well, Bibby Sterilin Ltd., UK) at 100 μl aliquots/well followed by 5 min centrifugation (900 ×*g*, Sigma 2–16 K). The culture medium was changed every two days and aggregate/EB formation was observed between 2 and 4 days after initial seeding and centrifugation.

2.4. Incorporation of microparticles into EBs

Incorporation of MPs within EBs was accomplished by coating MPs with HUES-7 cell lysate. In brief, using a haemocytometer, 5×10^5 MPs were suspended in 1 ml PBS containing HUES-7 cell lysate from 1×10^6 cell. The final suspension was then mixed gently and left on a roller mixer for 2 h before use. Aggregation was performed in a 96 multi-well plate with V-shaped bottom (Sero-Well, Bibby Sterilin Ltd., UK) as described above at 50:1 cell to MP ratio.

Using Nikon stereomicroscope SMZ 1500 which allowed bright field as well as fluorescent image capturing, coumarin-6 labelled MPs appearing in green were counted visually for each cell pellet. The distribution and localisation of PLGA MPs within multi-cellular EB model were studied using confocal microscopy (Leica SP2). Image analysis and Z stacking over a 10 μm optical section was accomplished using Velocity 5 software.

Experimental groups included EBs with MPs loaded with either BMP2, simvastatin pro-drug or active drug. Control groups included EBs with blank MPs or EBs without MPs.

Cell culture medium used for experimentation was MEF cell conditioned medium, without any other factors other than released from the MPs as described earlier.

2.5. Real time QPCR for osteocalcin

All cultures were lysed and RNA extracted using a Qiagen RNeasy mini kit (Qiagen, UK). RNA was quantified using a Nanodrop (Labtech, UK). Samples were reverse transcribed into cDNA using superscript III system (Invitrogen, UK). In brief, this included, mixing of 1 μl of 10 mM dNTP (Roche Applied Science) and 1 μl of random hexamer (250 ng/μl) (Invitrogen, UK) in addition to 11 μl of molecular biology grade water (Sigma-Aldrich, UK) containing 100 ng total RNA. The reaction mix was then transferred to a thermocycler (PX2) and incubated at 65 °C for 5 min to allow denaturation before quenching on ice for 1 min. Reaction Master Mix consisting of 4 μl of the first strand buffer, 1 μl of DTT, 1 μl of RNase-OUT and 1 μl of superscript III enzyme was prepared and added to the reaction mix after cooling of samples. With a final volume of 20 μl of sample, reverse transcription was started by incubation in thermo-cycler for 5 min at 25 °C then 60 min at 55 °C and finally the reaction was ended by heating for 15 min at 70 °C. qPCR was followed using Taqman Probes for *osteocalcin* and *GAPDH* (Applied Biosystems, UK).

2.6. Osteocalcin ELISA

Cell culture supernatant from different groups was first purified using special protein collection column (Millipore, UK). Samples were spun for 30 min (14,000 ×*g*, Sigma 1-16Ke) then follow through discarded and purified samples were collected from the membrane. Quantification of OCN was done using an ELISA kit from Bender Medsystems, Austria. 100 μl of distilled water plus 25 μl of each sample were added to a separate micro-plate wells. These were pre-coated with monoclonal mouse antibody against human OCN and also contained a lyophilised HRP-conjugate which is murine anti-human OCN monoclonal antibody. Incubation continued for 2 h at room temperature before washing. Then a 100 μl/well of substrate solution (tetramethylbenzidine) was added to samples followed by incubation for 15 min at room temperature (protected from light). Finally, 100 μl of a stop solution consisting of 1 M phosphoric acid was added and the optical density (OD) was measured at 450 nm using multimode micro-plate reader (Tecan Infinite 200, Switzerland). The experiment was repeated two times with a total of six replicates. Statistical analysis for sample replicates was followed using GraphPad InStat version 3.0 (GraphPad Software Inc.). Data analysis used the unpaired *t* test for parametric data sets and results were considered significant when $P < 0.05$ (*), very significant when $P < 0.01$ (**) and extremely significant when $P < 0.001$ (***).

2.7. Immunostaining

Staining for OCN and/or RUNX-2 was performed on samples fixed in a 4% (w/v) solution of para-formaldehyde (Sigma-Aldrich, UK) in PBS for 15 min then washed with PBS for 5 min. A mouse staining kit (R&D, UK) was used for detecting OCN staining and a goat staining kit was used for Runx-2 (R&D, UK). Endogenous peroxidase was exhausted by incubation with 3% hydrogen peroxide in PBS for 5 min. Samples were then washed with PBS buffer for 5 min before incubation with serum blocking for 15 min. Incubation was followed with avidin blocking reagent for another 15 min then rinsed with PBS buffer and drained from excess moisture. The latter step was repeated with biotin blocking reagent. Samples were then incubated overnight (2–8 °C) with the primary antibody solution (10 μg/ml) which was goat anti-human RUNX-2 antibody (R&D UK) or murine anti-human OCN antibody (R&D UK). On the following day, samples were rinsed with PBS for 15 min then drained from excess moisture before incubation with the biotinylated secondary antibody for 60 min. This was followed by washing with PBS for 15 min and drained samples were then incubated with high sensitivity streptavidin-horse radish peroxidase conjugate (HSS-HRP) for 30 min. A brief PBS washing steps for 2 min was then followed by incubation with 3,3-diaminobenzidine (DAB) chromagen solution for up to 20 min. Then after, samples were washed with distilled water and mounted with ProLong Gold antifade reagent with DAPI (Invitrogen, UK) and stored in the dark at 4 °C until microscopic examination. Technical controls were always used to exclude non-specific binding of the secondary antibody.

2.8. Histology

Alizarin red (AR) staining for calcium and matrix mineralisation was done by first washing samples with PBS followed by fixation in 4% (w/v) para-formaldehyde (Sigma-Aldrich, UK) in PBS for approximately 30 min. A second washing step with deionised water was followed before staining with 1% AR (w/v) (Sigma-Aldrich, UK) in deionised water, pH 4.2 for 5 min at room temperature. The cell preparations were washed five times with deionised water until the water became clear.

Demonstration of collagen was done by staining with a 0.1% solution of picrosirus red in saturated aqueous picric acid (VWR, UK). Samples were incubated at room temperature for 40 min before brief washing with water then industrial methylated spirit and finally mounting in PBS:glycerol (1:1) before imaging.

3. Results

3.1. 3D model of hES cell derived EBs containing MPs

Incorporation of P_{DL}LGA MPs within the multicellular structure of human ES cell-derived EBs was done by forced aggregation via centrifugation. Different cell to MP ratios ranging from 50:1 to 3000:1 were investigated. The incorporation of a defined number of MPs within the cell pellet was successful as shown in Table 1. HUES-7 cells have no affinity toward P_{DL}LGA MPs as suggested by the observation, where despite the presence of MPs within the cell pellets on day zero of aggregation, by day two most of the MPs had been expelled from the EBs. Only sporadic replicates revealed a few MPs retained on the periphery of the EBs on day 4 as shown in Fig. 1(A). This kind of sporadic, unpredictable aggregation will not be of value in establishing a reliable 3D model of HUES-7 cell aggregate with P_{DL}LGA MPs. Marked improvement with MP incorporation within hES cell-derived EBs was achieved by suspending the MPs in HUES-7 cell lysate solution prior to the aggregation process. Results from this approach appeared to be successful

Table 1
The incorporation of a definable number of HUES-7 cell lysate coated P_{DL}LGA MPs with HUES-7 cell pellet at different cell to MPs ratio.

The cell/MP ratio	Predicted MP number within 3×10^3 cell pellet	Actual MP number within 3×10^3 cell pellet
50 to 1	60	59 (±7.5)
100 to 1	30	23 (±1)
300 to 1	10	10 (±1.6)
500 to 1	6	5 (±0.6)
1000 to 1	3	4 (±0.3)
3000 to 1	1	2 (±0.4)

Values of actual MP incorporation were expressed as mean ± SEM from 5 to 9 replicates.

with a marked improvement in the retention of MPs within EBs as shown in Fig. 1B; these MPs remained within EBs until day 21 as confirmed in Fig. 2A.

Time lapse microscopy imaging for HUES-7 derived EBs between day two and three post aggregation revealed dynamic movement within the aggregate as shown in the Supplementary movie (S2).

3.2. P_{DL}LGA MPs as a release model for EBs

The application of P_{DL}LGA MPs as a release model within EBs was tested using P_{DL}LGA MPs loaded with CellTracker red. The results were consistent with time lapse video observations described above, with dynamic movement within the EB structure (Fig. 2A). MPs appeared to be located around the centre of the EB until day 7 (Fig. 2A1and A2) then became more dispersed throughout the EB by day 14 (Fig. 2A3). MPs remained within the EBs until the end of the study on day 21 (Fig. 2A4). The distribution of the MPs within EBs was confirmed from reconstructed z-stack images collected by confocal microscopy (Fig. 2B and the Supplementary movies S3 and S4). There was an interesting pattern of release and diffusion of the encapsulated CellTracker red from the MPs within the multi-cellular EB structure as shown in Fig. 2A. The diffusion of the red fluorescence was limited within the EB structure on day 4 and became more uniform by days 7, 14 and 21 with whole EB showing red fluorescence.

3.3. Simvastatin and /or BMP-2 loaded MP model

A 3D model of HUES-7-derived EBs containing P_{DL}LGA MPs loaded with simvastatin pro-drug or simvastatin active drug or BMP-2 was tested for osteogenic differentiation for up to 21 days in culture. Examples of release profiles of the encapsulated molecule(s) can be seen in Supplementary Fig. 5.

3.3.1. Osteocalcin gene expression

Real time quantitative PCR was used to measure the difference in the gene expression of OCN (late marker for osteogenesis) relative to GAPDH gene expression. The relative OCN expression was quantified on days 7, 14 and 21 as fold change in relation to a reference group of day 21 EBs without MPs. As shown in Fig. 3A, there was a comparable up-regulation in OCN expression on day 21 by around 2 fold with MPs loaded with each one of the following; simvastatin prodrug, simvastatin active drug and BMP-2. EBs containing blank MPs showed a 1.57 fold increase in OCN expression on day 21; however OCN expression was detected on day 21 but not days 7 and 14 with EBs without MPs and EBs containing blank MPs.

3.3.2. Osteocalcin protein release

The ELISA OCN protein release assay revealed similar but modest increases in the level OCN secreted into the culture medium (Fig. 3B); simvastatin pro-drug 2.44 (±0.07 ng/ml), simvastatin active drug 2.36 (±0.032 ng/ml) and BMP-2 2.42 (±0.04 ng/ml). These increases were significant when compared against control experiments which included EBs containing MPs without any loaded drugs or cytokines and particularly for EBs without MPs.

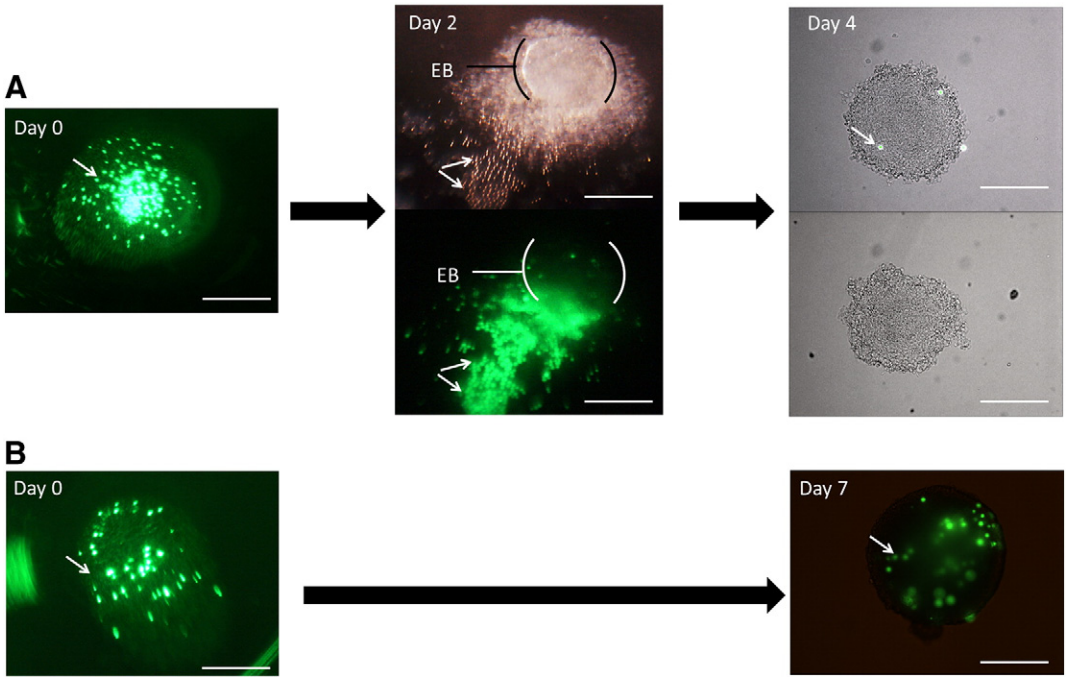

Fig. 1. Representative microscopic image for HUES-7 EBs/P_{DL}LGA MPs aggregate with arrows referring to the MPs. A) — The incorporation of the P_{DL}LGA MPs within EBs from day zero (MPs within the cell pellet) and day 2 with most of the MPs expelled out of the EB followed by day 4 showing EBs with or without superficially attached MPs. B) — Cell lysate coated P_{DL}LGA MP integration within EB multicellular structure, these MPs were retained with EBs between day zero and day 7. Scale bar equals to 500 um.

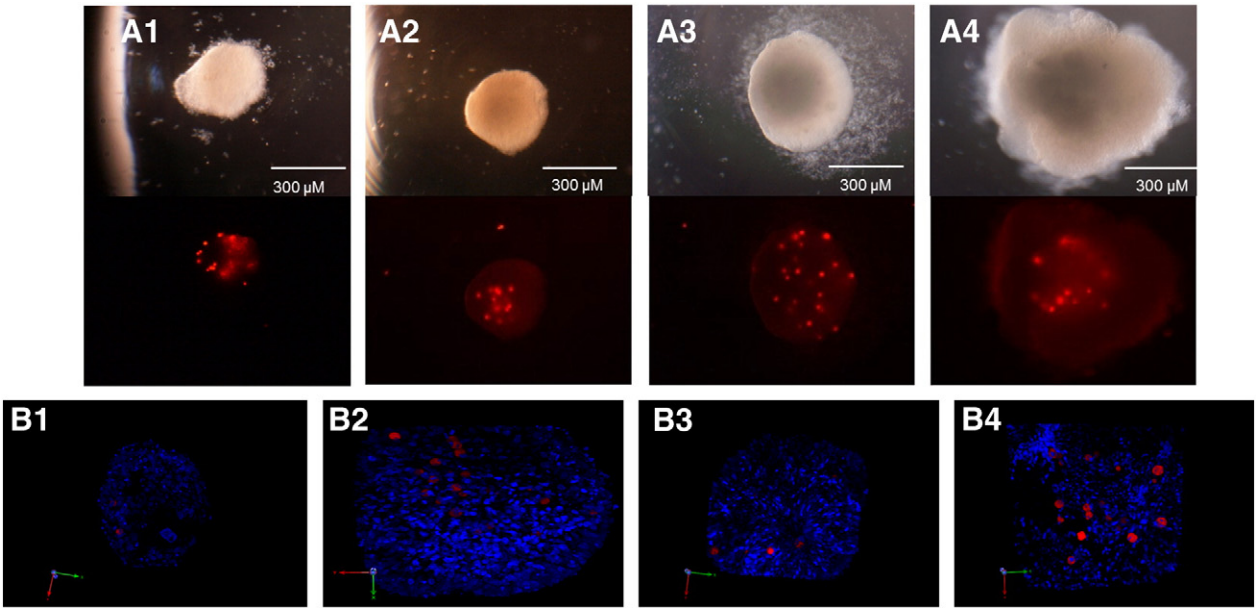

Fig. 2. Representative microscopic images for HUES-7 EBs/P_{DL}LGA MP aggregate. A) HUES7 cell lysate treated MPs, A1–A4 are bright field images (top) and fluorescent images for MPs labelled with CellTracker red (bottom). Cell number per EB was 3×10^3 cells per well with 50:1 cell–MPs ratio. MPs can be seen fluorescing with CellTracker red on days 4 (A1), 7 (A2), 14 (A3) and 21 (A4). Finally, B) Confocal microscopy images (40×) for HUES-7 EBs stained with DAPI nuclear stain appear with P_{DL}LGA MPs labelled with CellTracker red at different time points (B1 — day 2, B2 — day 7, B3 — day 14 and B4 — day 17).

3.3.3. RUNX-2 and osteocalcin protein expression

3.3.3.1. RUNX2. The presence of RUNX-2 (early osteogenic marker) in EBs containing MPs loaded with simvastatin (pro or active drug) and/or BMP-2 was compared against control group of EBs containing blank MPs and/or EBs without MPs. Results revealed a comparable weak positive staining (light brown) with both control groups containing blank MPs or devoid from MPs on day 7. A most and comparable level of staining was seen within EBs containing MPs with either form pro and active drug forms of simvastatin (see the Supplementary Fig. 6).

3.3.3.2. Osteocalcin. Results of OCN immunostaining was consistent with observations on OCN gene expression with no evidence of staining on day 7 (Fig. 4A), however, weak positive staining was evident on day 21 in EBs without MPs and similarly within EBs containing blank MPs as seen in Fig. 4B. More intense staining for OCN was evident within EBs containing MPs loaded with BMP2 (Fig. 4B3) and/or simvastatin active drug (Fig. 4B3) and/or simvastatin prodrug (Fig. 4B5). Furthermore, MPs could be readily identified within EBs and it was possible to locate zones of positive staining for OCN around MPs embedded within EBs (Supplementary Fig. 7).

3.3.3.3. Histochemical staining for collagen and calcium/mineral deposition. Collagen formation was investigated by picrosirius red staining, which can be used to distinguish collagens. All groups of EBs showed evidence for picrosirius red staining (Fig. 5A) within the EBs. Staining for picrosirius red appeared more intense and homogeneous in day 21 EBs with MPs containing BMP-2, simvastatin active drug or simvastatin pro-drug.

Calcium and mineralisation within EBs were assessed by Alizarin red staining and there was no evidence of staining in any of the groups under test on day 14 (Fig. 5B). By day 21 small areas of staining were evident in EBs without MPs and EBs with blank MPs (Fig. 5B1a and B2a). Appreciably more Alizarin red staining was seen in EBs with MPs containing BMP-2 (Fig. 5B3a), simvastatin active drug (Fig. 5B4a) or simvastatin pro-drug (Fig. 5B5a) and was similar between each group in terms of distribution and intensity of staining.

3.4. VEGF loaded MPs

There was no evidence of immunostaining for CD31 PECAM revealed in any of the EB groups on day 7 (Fig. 6). By day 14 there was obvious staining for CD31 only in EBs VEGF MPs, which became more prominent by days 21 and 28 and eventually spreading throughout the whole EB.

4. Discussion

In this study we demonstrate an effective and efficient approach for incorporating defined numbers of MPs within human ES cell derived aggregates. Moreover, by incorporating simvastatin pro or active drug or BMP2 or VEGF into the MPs we show localised osteogenic and vascular differentiation within the cellular aggregates. This provides a powerful tool for controlling and investigating differentiation within 3D cell cultures and has applications for drug delivery, drug discovery, stem cell biology, tissue engineering and regenerative medicine.

In recent years there has been much interest in developing 3D cell models with controlled release of cytokines or drugs from MPs within those models. Important considerations for creating successful 3D models require attention to the incorporation of MPs within the multicellular EB structure and should enable reliable distribution and a release pattern of the encapsulated molecule of interest in a sustained and predictable manner. Ferreira, Squier, Park, Choe, Kohane, and Langer in 2008 incorporated MPs successfully within human ES cell-derived EB by suspending MPs as mg/ml preparation in culture medium with ES cells before centrifugation [34]. Rotary orbital culture has also been used for incorporating MPs within EBs [33,35]. In a more recent study, Bratt-Leal, Carpenedo, Ungrin, Zandstra, and McDevitt in 2011 demonstrated a more efficient incorporation of MPs within EBs using a forced aggregation method and directly when compared against rotary orbital culture [40]. While previous studies have reported successful incorporation of MPs into EBs, the level of control of numbers of MPs has been variable, ranging from a minimum of less than 100 MPs/EB and a maximum of up to 600 MPs per EB. Such variability is likely to affect both amounts of the drug or cytokine delivered and subsequent cell responses. The aim

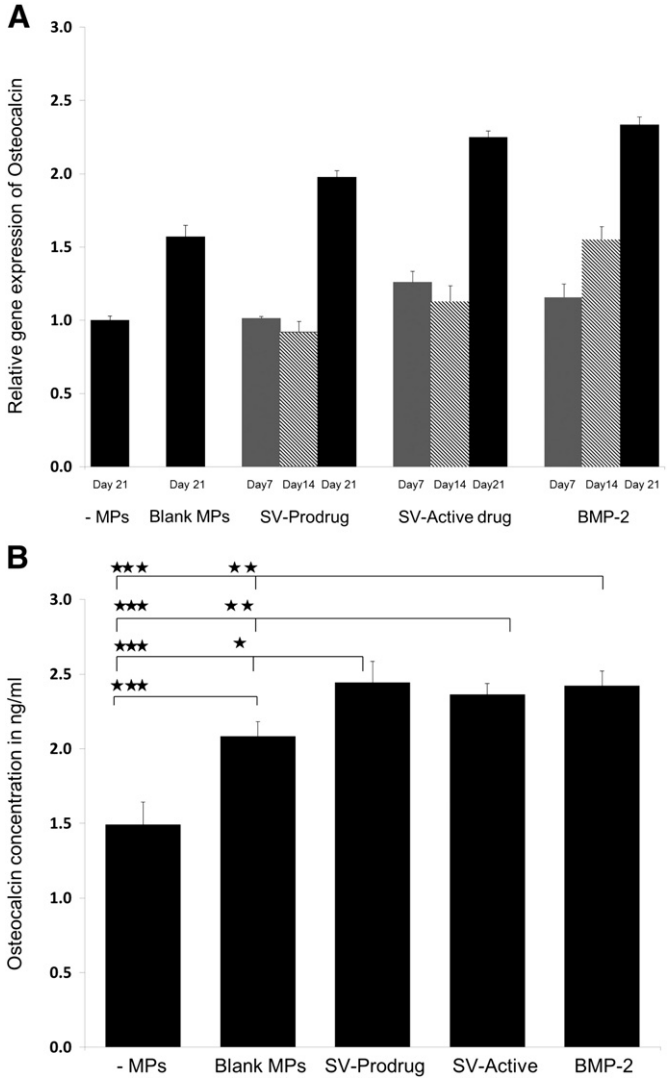

Fig. 3. A) — Relative expression of OCN to GAPDH in HUES-7-derived EBs containing MPs loaded with either 0.1% BMP-2, 0.5% simvastatin prodrug or active drug or blank MPs. Gene expression was quantified on days 7, 14, 21 and presented as fold change in relation to reference of day 21 EBs devoid from MPs as mean ± SEM (n = 2 and r = 3). B) Secreted human OCN protein levels in HUES-7-derived EBs on day 21. Results expressed as Mean ± SEM of 6 determinations. Differences considered significant (*) when $P < 0.05$, highly significant (**) when $P < 0.01$ and extremely significant (***) when $P < 0.001$.

of this study was to provide much more controlled incorporation of MPs within EBs, down to 10 or fewer MPs per EB and thereby provide minimal disruption to EBs integrity and cell interactions and enable better investigation of the effects of low, local concentrations of the released molecule of interest.

One of the challenges for introducing $P_{DL}LGA$ MPs into cellular aggregates is the hydrophobicity of the polymer surface and its poor wettability, which can hinder cell attachment [36]. Furthermore, cells within the early embryo can be highly mobile [53]. Cell mobility and MP movement were seen in this study and offer an explanation for initial failed attempts to achieve precise control in terms of MP number within ES cell pellet pre-aggregation and loss of MPs from within EBs post aggregation. Improved cell interaction and attachment to polymer surfaces can be achieved by changing surface roughness using ethanol or sodium hydroxide [36,54] or via coating with different materials like collagen, gelatine, and agarose [33,35,40,41]. However, variability related to the coating material has been reported [40]. For these reasons in the present work, marked improvement of MP incorporation with EBs was achieved following coating of MPs with hES cell lysate. Although coating could have an influence on the release profile of the molecules of interest, on the other hand the results demonstrated accuracy for the incorporation of $P_{DL}LGA$ MPs within EBs down to one MP per EB. The model was stable with MPs still detectable at different regions within the EBs throughout the 21 days of the study confirming retention of the incorporated MPs and the overall reliability of this delivery method. The mechanisms contributing to improved incorporation and retention of MPs within EBs by prior coating with hES cell lysate remains to be investigated, although using lysate from the same cell source as those contributing to the formation of the cell aggregate might improve compatibility.

Following on from creating a reliable and controllable incorporation of $P_{DL}LGA$ MPs within hES cell derived EBs, the release profile of the CellTracker red MPs and progressive distribution of the dye throughout EBs over time demonstrated the efficacy of the model for future applications with controlled release bioactive molecules. This also facilitated demonstration of our approach to deliver drug molecules and cytokines. The release pattern started with an initial burst followed by a decline phase which entered a steady state release with both forms of simvastatin. Unlike the statins, BMP-2 release started with an initial burst then followed by a steady state release. In this study we chose to investigate delivery of simvastatin pro- and active drugs and BMP2 as known inducers of osteogenesis [55] and also VEGF as an inducer of vasculogenesis [56]. The efficient diffusion of CellTracker red can be facilitated by a combined effect from an initial burst release and highly mobile MPs within an EB which can add to the model reliability for efficient delivery of the molecule of interest.

Induction of osteogenic differentiation involves *Runx-2* up-regulation, which is a key transcription factor during osteogenesis [57–59]. *Runx-2* is believed to be an upstream regulator for *Osterix* [60] and is also responsible for regulating *ALP*, *OCN*, *osteopontin*, *collagen-I* and *BSP* expression, however its expression is transient [59,61–66]. OCN tends to show up-regulation associated with ECM formation and mineral deposition and is considered a comparatively late marker of end stage osteogenic differentiation [67]. Therefore OCN was considered a useful marker for evaluating the 3D-MPs model for osteogenesis and to also demonstrate stability of the model over 21 days. Results in this study showed a time dependent expression of *OCN* with the highest level seen at day 21 and was consistent and comparable for simvastatin pro- and active drugs and BMP-2, with a negligible expression in EBs without MPs or with blank MPs. Staining for Runx-2 protein suggested a higher expression in EBs containing $P_{DL}LGA$ MPs loaded with either forms of simvastatin, however a weaker expression was noticed with the BMP-2 group and could relate to an earlier expression of this temporally expressed early marker during osteogenesis. Osteogenic differentiation was further confirmed by OCN protein release detected by OCN ELISA and these results were consistent with the *OCN* gene expression data. OCN was also detected within the EBs by immunostaining and robust staining was seen in EBs containing MPs loaded with simvastatin pro or active drugs or BMP-2, with localised zones of staining associated with MPs within the EBs. Consistent findings were also seen for the major ECM protein (collagen). The latter stages of osteogenesis typically involve matrix mineralisation [68] which was not evident in this study until day 21 with appreciably higher levels of calcium deposition and suggested mineralisation within EBs containing MPs loaded with either forms of simvastatin or BMP-2.

From these studies it was noted that while the best evidence for osteogenesis was supported from observations using MPs releasing known osteogenic drugs and cytokines there was still evidence of osteogenesis within EBs containing blank MPs particularly when compared with EBs without MPs. Several studies have reported important contributions from surface chemistry and micro-topography on osteogenesis [69–74] and Scaglione, Braccini, Wendt, Jaquiery, Beltrame, Quarto, and Martin in 2006 demonstrated osteogenesis on a 3D ceramic scaffold in the absence of defined osteo-inductive molecules [75]. This together

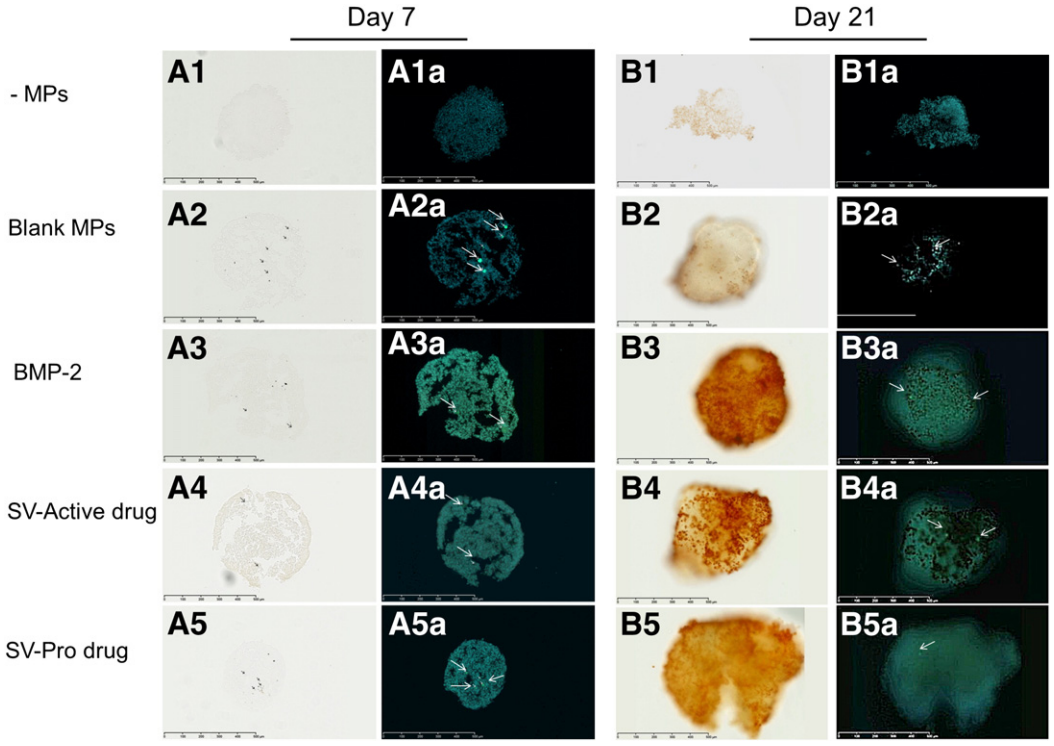

Fig. 4. Immunostaining for OCN in day 7 EBs (A1–A5) and day 21 EBs (B1–B5), positive results appear in brown, samples were counterstained with DAPI nuclear staining (appeared with blue fluorescence) with arrows showing MPs. EBs without MPs (A1 and B1) and EBs with blank MPs (A2 and B2). BMP-2 loaded MPs (A3 and B3), simvastatin active drug MPs (A4 and B4) and simvastatin pro-drug loaded MPs (A5 and B5).

with the physical presence of the polymer MPs could help explain the small amount of osteogenesis seen within EBs containing MPs without any drug molecules or cytokines.

As a further example of the applications of this MP delivery method we also demonstrated differentiation of endothelial cells, based on CD31 PECAM, within EBs containing VEGF MPs. Related on-going

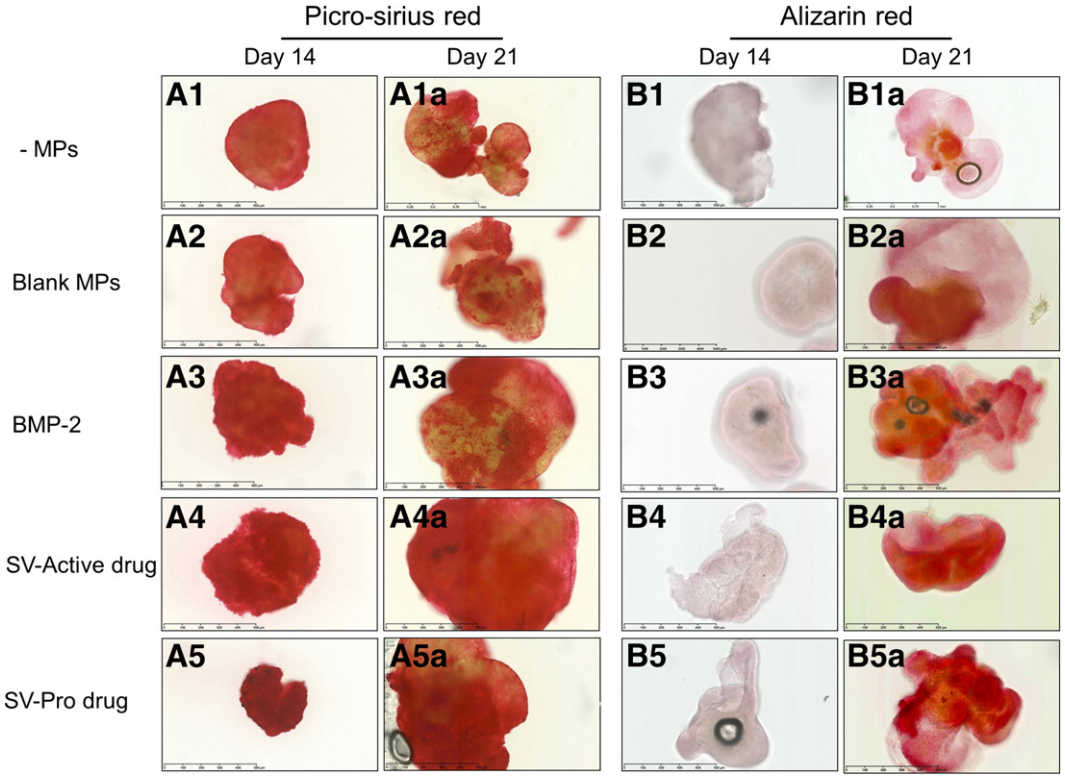

Fig. 5. Representative microscopy images of EBs stained with picrosirius red (left panels) on day 14 (A1–A5) and day 21 (A1a–A5a) and EBs stained with Alizarin red (right panels) on day 14 (B1–B5) and day 21(B1a–B5a). Positive results appear in bright red staining; (A1 and B1) EBs without MPs; (A2 and B2) EBs with blank MPs; (A3 and B3) EBs with BMP-2 MPs; (A3 and B3) simvastatin active drug MPs and; (A5 and B5) simvastatin pro-drug MPs.

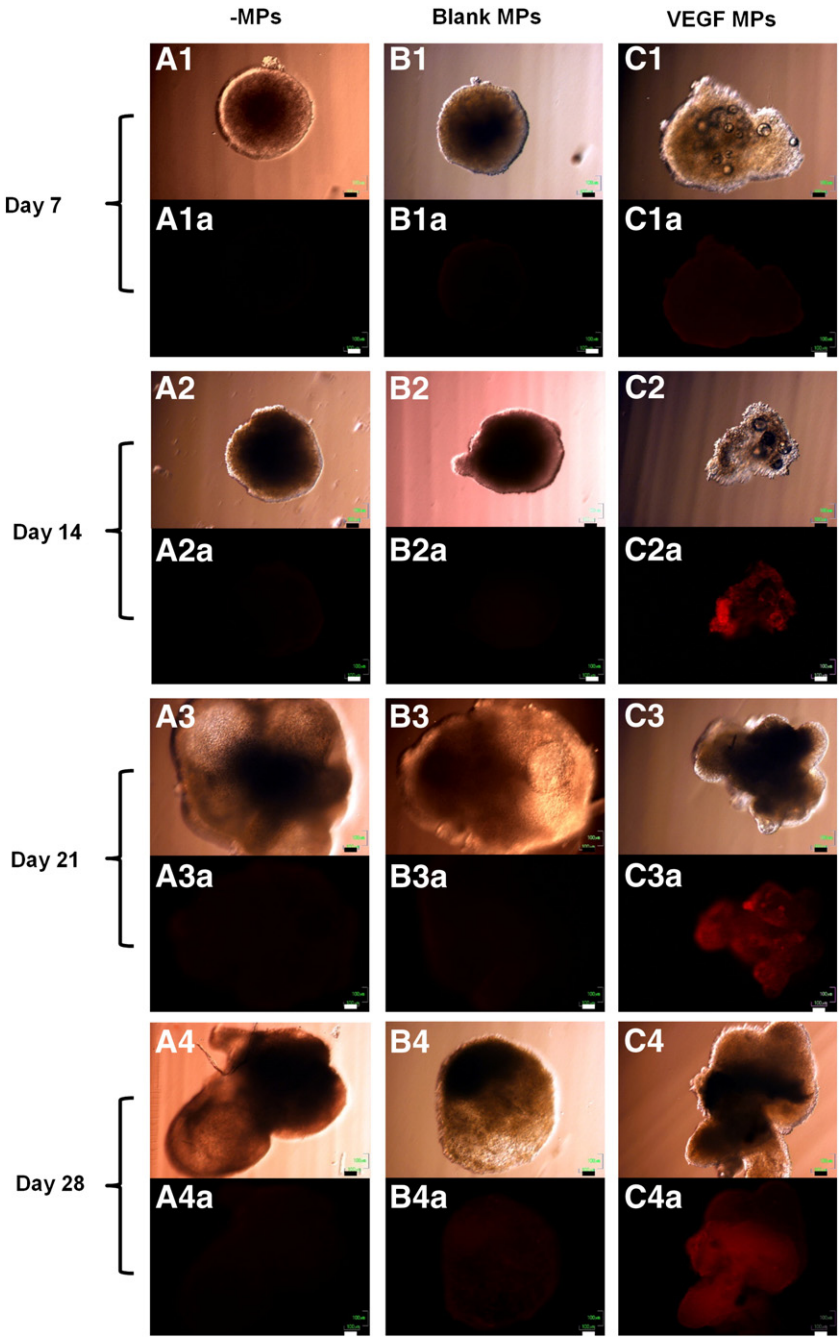

Fig. 6. Representative bright field and fluorescence microscopy images of days 7, 14, 21 and 28 HUES-7 EBs stained with CD31 PECAM. Positive results appear in red. A — EBs without MPs. B — EBs with blank MPs. C — EBs with 0.1% VEGF MPs.

work is exploring approaches to engineer cell aggregates to contain MPs with different drugs/cytokines and to facilitate co-ordinated delivery of multiple signals within 3D cell aggregates.

5. Conclusion

Work presented in this study succeeded in establishing an effective method for introducing and retaining definable numbers of MP human ES cell-derived 3D multicellular aggregates. We also demonstrate the capacity for these MPs to deliver drug molecules and cytokines directly within the cellular aggregates and as specifically investigated here using simvastatin, BMP2 and VEGF facilitating localised osteogenic or vasculogenic differentiation. This approach can help to overcome the limitations associated with the many current models of ensuring efficient directed delivery of drugs or cytokines to and within 3D cell culture models and has wide applications in drug delivery and regenerative medicine.

Supplementary data to this article can be found online at http://dx.doi.org/10.1016/j.jconrel.2013.02.029.

Acknowledgements

Dr Glen Kirkham and Dr Lloyd Hamilton are thanked for their many helpful discussions.

References

[1] H.L. Ashe, J. Briscoe, The interpretation of morphogen gradients, Development 133 (2006) 385–394.
[2] J.B. Gurdon, P.Y. Bourillot, Morphogen gradient interpretation, Nature 413 (2001) 797–803.

[3] Y. Saka, J.C. Smith, A mechanism for the sharp transition of morphogen gradient interpretation in *Xenopus*, BMC Dev. Biol. 7 (2007) 47.
[4] T. Tabata, Y. Takei, Morphogens, their identification and regulation, Development 131 (2004) 703–712.
[5] K.M. Cadigan, Regulating morphogen gradients in the *Drosophila* wing, Semin. Cell Dev. Biol. 13 (2002) 83–90.
[6] S.R. Yu, M. Burkhardt, M. Nowak, J. Ries, Z. Petrasek, S. Scholpp, P. Schwille, M. Brand, Fgf8 morphogen gradient forms by a source-sink mechanism with freely diffusing molecules, Nature 461 (2009) 533–536.
[7] L. Wolpert, Positional information and the spatial pattern of cellular differentiation, J. Theor. Biol. 25 (1969) 1–47.
[8] K. Ogawa, Y. Miyake, Generation model of positional values as cell operation during the development of multicellular organisms, Biosystems 103 (2010) 400–409.
[9] A. Birgersdotter, R. Sandberg, I. Ernberg, Gene expression perturbation in vitro — a growing case for three-dimensional (3D) culture systems, Semin. Cancer Biol. 15 (2005) 405–412.
[10] S. Ghosh, G.C. Spagnoli, I. Martin, S. Ploegert, P. Demougin, M. Heberer, A. Reschner, Three-dimensional culture of melanoma cells profoundly affects gene expression profile: a high density oligonucleotide array study, J. Cell. Physiol. 204 (2005) 522–531.
[11] T.T. Chang, M. Hughes-Fulford, Monolayer and spheroid culture of human liver hepatocellular carcinoma cell line cells demonstrate distinct global gene expression patterns and functional phenotypes, Tissue Eng. Part A 15 (2009) 559–567.
[12] C.M. Gundberg, P.V. Hauschka, J.B. Lian, P.M. Gallop, Osteocalcin: isolation, characterization, and detection, Methods Enzymol. 107 (1984) 516–544.
[13] I. Grabowska, A. Szeliga, J. Moraczewski, I. Czaplicka, E. Brzoska, Comparison of satellite cell-derived myoblasts and C2C12 differentiation in two- and three-dimensional cultures: changes in adhesion protein expression, Cell Biol. Int. 35 (2010) 125–133.
[14] H.E. Brink, J. Bernstein, S.B. Nicoll, Fetal dermal fibroblasts exhibit enhanced growth and collagen production in two- and three-dimensional culture in comparison to adult fibroblasts, J. Tissue Eng. Regen. Med. 3 (2009) 623–633.
[15] J. Brennan, C.C. Lu, D.P. Norris, T.A. Rodriguez, R.S. Beddington, E.J. Robertson, Nodal signalling in the epiblast patterns the early mouse embryo, Nature 411 (2001) 965–969.
[16] U. Chen, M. Kosco, Differentiation of mouse embryonic stem cells in vitro: III. Morphological evaluation of tissues developed after implantation of differentiated mouse embryoid bodies, Dev. Dyn. 197 (1993) 217–226.
[17] C. Cerdan, S.H. Hong, M. Bhatia, Formation and hematopoietic differentiation of human embryoid bodies by suspension and hanging drop cultures, Curr. Protoc. Stem Cell Biol. 3 (2007) 1D.2.1–1D.2.16.
[18] W.T. Fung, A. Beyzavi, P. Abgrall, N.T. Nguyen, H.Y. Li, Microfluidic platform for controlling the differentiation of embryoid bodies, Lab Chip 9 (2009) 2591–2595.
[19] E.S. Ng, R. Davis, E.G. Stanley, A.G. Elefanty, A protocol describing the use of a recombinant protein-based, animal product-free medium (APEL) for human embryonic stem cell differentiation as spin embryoid bodies, Nat. Protoc. 3 (2008) 768–776.
[20] E.S. Ng, R.P. Davis, L. Azzola, E.G. Stanley, A.G. Elefanty, Forced aggregation of defined numbers of human embryonic stem cells into embryoid bodies fosters robust, reproducible hematopoietic differentiation, Blood 106 (2005) 1601–1603.
[21] L.D. Buttery, S. Bourne, J.D. Xynos, H. Wood, F.J. Hughes, S.P. Hughes, V. Episkopou, J.M. Polak, Differentiation of osteoblasts and in vitro bone formation from murine embryonic stem cells, Tissue Eng. 7 (2001) 89–99.
[22] V. Sottile, A. Thomson, J. McWhir, In vitro osteogenic differentiation of human ES cells, Cloning Stem Cells 5 (2003) 149–155.
[23] N.I. zur Nieden, G. Kempka, H.J. Ahr, In vitro differentiation of embryonic stem cells into mineralized osteoblasts, Differentiation 71 (2003) 18–27.
[24] T. Cao, B.C. Heng, C.P. Ye, H. Liu, W.S. Toh, P. Robson, P. Li, Y.H. Hong, L.W. Stanton, Osteogenic differentiation within intact human embryoid bodies result in a marked increase in osteocalcin secretion after 12 days of in vitro culture, and formation of morphologically distinct nodule-like structures, Tissue Cell 37 (2005) 325–334.
[25] G.R. Chaudhry, D. Yao, A. Smith, A. Hussain, Osteogenic cells derived from embryonic stem cells produced bone nodules in three-dimensional scaffolds, J. Biomed. Biotechnol. 2004 (2004) 203–210.
[26] Y.J. Ko, R.S. Zaharias, D.A. Seabold, J. Lafoon, G.B. Schneider, Osteoblast differentiation is enhanced in rotary cell culture simulated microgravity environments, J. Prosthodont. 16 (2007) 431–438.
[27] J. Karbanova, T. Soukup, J. Suchanek, J. Mokry, Osteogenic differentiation of human dental pulp-derived stem cells under various ex-vivo culture conditions, Acta Medica (Hradec Kralove) 53 (2010) 79–84.
[28] L.A. Smith, X. Liu, J. Hu, P.X. Ma, The enhancement of human embryonic stem cell osteogenic differentiation with nano-fibrous scaffolding, Biomaterials 31 (2010) 5526–5535.
[29] R. Langer, J.P. Vacanti, Tissue engineering, Science 260 (1993) 920–926.
[30] S. Cohen, T. Yoshioka, M. Lucarelli, L.H. Hwang, R. Langer, Controlled delivery systems for proteins based on poly(lactic glycolic acid) microspheres, Pharm. Res. 8 (1991) 713–720.
[31] Y.M. Wang, H. Sato, I. Horikoshi, In vitro and in vivo evaluation of taxol release from poly(lactic-co-glycolic acid) microspheres containing isopropyl myristate and degradation of the microspheres, J. Control. Release 49 (1997) 157–166.
[32] R.A. Jain, The manufacturing techniques of various drug loaded biodegradable poly(lactide-co-glycolide) (PLGA) devices, Biomaterials 21 (2000) 2475–2490.
[33] R.L. Carpenedo, A.M. Bratt-Leal, R.A. Marklein, S.A. Seaman, N.J. Bowen, J.F. McDonald, T.C. McDevitt, Homogeneous and organized differentiation within embryoid bodies induced by microsphere-mediated delivery of small molecules, Biomaterials 30 (2009) 2507–2515.
[34] L. Ferreira, T. Squier, H. Park, H. Choe, D.S. Kohane, R. Langer, Human embryoid bodies containing nano- and microparticulate delivery vehicles, Adv. Mater. 20 (2008) 2285.
[35] R.L. Carpenedo, S.A. Seaman, T.C. McDevitt, Microsphere size effects on embryoid body incorporation and embryonic stem cell differentiation, J. Biomed. Mater. Res. A 94 (2010) 466–475.
[36] A.G. Mikos, M.D. Lyman, L.E. Freed, R. Langer, Wetting of poly(L-lactic acid) and poly(DL-lactic-co-glycolic acid) foams for tissue culture, Biomaterials 15 (1994) 55–58.
[37] H. Zhu, J. Ji, R. Lin, C. Gao, L. Feng, J. Shen, Surface engineering of poly(D,L-lactic acid) by entrapment of chitosan-based derivatives for the promotion of chondrogenesis, J. Biomed. Mater. Res. 62 (2002) 532–539.
[38] J. Yang, G. Shi, J. Bei, S. Wang, Y. Cao, Q. Shang, G. Yang, W. Wang, Fabrication and surface modification of macroporous poly(L-lactic acid) and poly(L-lactic-co-glycolic acid) (70/30) cell scaffolds for human skin fibroblast cell culture, J. Biomed. Mater. Res. 62 (2002) 438–446.
[39] Y.L. Cui, A.D. Qi, W.G. Liu, X.H. Wang, H. Wang, D.M. Ma, K.D. Yao, Biomimetic surface modification of poly(L-lactic acid) with chitosan and its effects on articular chondrocytes in vitro, Biomaterials 24 (2003) 3859–3868.
[40] A.M. Bratt-Leal, R.L. Carpenedo, M.D. Ungrin, P.W. Zandstra, T.C. McDevitt, Incorporation of biomaterials in multicellular aggregates modulates pluripotent stem cell differentiation, Biomaterials 32 (2011) 48–56.
[41] S.K. Sahoo, A.K. Panda, V. Labhasetwar, Characterization of porous PLGA/PLA microparticles as a scaffold for three dimensional growth of breast cancer cells, Biomacromolecules 6 (2005) 1132–1139.
[42] S. Miyatani, K. Shimamura, M. Hatta, A. Nagafuchi, A. Nose, M. Matsunaga, K. Hatta, M. Takeichi, Neural cadherin: role in selective cell–cell adhesion, Science 245 (1989) 631–635.
[43] M.J. Mahoney, W.M. Saltzman, Transplantation of brain cells assembled around a programmable synthetic microenvironment, Nat. Biotechnol. 19 (2001) 934–939.
[44] M. Balcells, E.R. Edelman, Effect of pre-adsorbed proteins on attachment, proliferation, and function of endothelial cells, J. Cell. Physiol. 191 (2002) 155–161.
[45] A. Kikuchi, H. Taira, T. Tsuruta, M. Hayashi, K. Kataoka, Adsorbed serum protein mediated adhesion and growth behavior of bovine aortic endothelial cells on polyamine graft copolymer surfaces, J. Biomater. Sci. Polym. Ed. 8 (1996) 77–90.
[46] P.B. van Wachem, C.M. Vreriks, T. Beugeling, J. Feijen, A. Bantjes, J.P. Detmers, W.G. van Aken, The influence of protein adsorption on interactions of cultured human endothelial cells with polymers, J. Biomed. Mater. Res. 21 (1987) 701–718.
[47] S.P. Massia, J.A. Hubbell, Covalently attached GRGD on polymer surfaces promotes biospecific adhesion of mammalian cells, Ann. N. Y. Acad. Sci. 589 (1990) 261–270.
[48] S.P. Massia, J.A. Hubbell, Human endothelial cell interactions with surface-coupled adhesion peptides on a nonadhesive glass substrate and two polymeric biomaterials, J. Biomed. Mater. Res. 25 (1991) 223–242.
[49] N.M. Green, Avidin, Adv. Protein Chem. 29 (1975) 85–133.
[50] M.P. Desai, V. Labhasetwar, E. Walter, R.J. Levy, G.L. Amidon, The mechanism of uptake of biodegradable microparticles in Caco-2 cells is size dependent, Pharm. Res. 14 (1997) 1568–1573.
[51] K.Y. Win, S.S. Feng, Effects of particle size and surface coating on cellular uptake of polymeric nanoparticles for oral delivery of anticancer drugs, Biomaterials 26 (2005) 2713–2722.
[52] G.T.S. Kirby, L.J. White, C.V. Rahman, H.C. Cox, O. Qutachi, F.R.A.J. Rose, D.W. Hutmacher, K.M. Shakesheff, M.A. Woodruff, PLGA-based microparticles for the sustained release of BMP-2, Polymers 3 (2011) 571–586.
[53] C. Chazaud, Y. Yamanaka, T. Pawson, J. Rossant, Early lineage segregation between epiblast and primitive endoderm in mouse blastocysts through the Grb2–MAPK pathway, Dev. Cell 10 (2006) 615–624.
[54] G.E. Park, M.A. Pattison, K. Park, T.J. Webster, Accelerated chondrocyte functions on NaOH-treated PLGA scaffolds, Biomaterials 26 (2005) 3075–3082.
[55] T.T. Tang, B. Lu, B. Yue, X.H. Xie, Y.Z. Xie, K.R. Dai, J.X. Lu, J.R. Lou, Treatment of osteonecrosis of the femoral head with hBMP-2-gene-modified tissue-engineered bone in goats, J. Bone Joint Surg. Br. 89B (2007) 127–132.
[56] F.R. Formiga, B. Pelacho, E. Garbayo, G. Abizanda, J.J. Gavira, T. Simon-Yarza, M. Mazo, E. Tamayo, C. Jauquicoa, C. Ortiz-de-Solorzano, F. Prosper, M.J. Blanco-Prieto, Sustained release of VEGF through PLGA microparticles improves vasculogenesis and tissue remodeling in an acute myocardial ischemia–reperfusion model, J. Control. Release 147 (2010) 30–37.
[57] C. Banerjee, L.R. McCabe, J.Y. Choi, S.W. Hiebert, J.L. Stein, G.S. Stein, J.B. Lian, Runt homology domain proteins in osteoblast differentiation: AML3/CBFA1 is a major component of a bone-specific complex, J. Cell. Biochem. 66 (1997) 1–8.
[58] P. Ducy, M. Starbuck, M. Priemel, J. Shen, G. Pinero, V. Geoffroy, M. Amling, G. Karsenty, A Cbfa1-dependent genetic pathway controls bone formation beyond embryonic development, Genes Dev. 13 (1999) 1025–1036.
[59] P. Ducy, R. Zhang, V. Geoffroy, A.L. Ridall, G. Karsenty, Osf2/Cbfa1: a transcriptional activator of osteoblast differentiation, Cell 89 (1997) 747–754.
[60] K. Nakashima, X. Zhou, G. Kunkel, Z. Zhang, J.M. Deng, R.R. Behringer, B. de Crombrugghe, The novel zinc finger-containing transcription factor osterix is required for osteoblast differentiation and bone formation, Cell 108 (2002) 17–29.
[61] H. Harada, S. Tagashira, M. Fujiwara, S. Ogawa, T. Katsumata, A. Yamaguchi, T. Komori, M. Nakatsuka, Cbfa1 isoforms exert functional differences in osteoblast differentiation, J. Biol. Chem. 274 (1999) 6972–6978.
[62] R. Shen, X. Wang, H. Drissi, F. Liu, R.J. O'Keefe, D. Chen, Cyclin D1-cdk4 induce runx2 ubiquitination and degradation, J. Biol. Chem. 281 (2006) 16347–16353.
[63] R.T. Franceschi, G. Xiao, Regulation of the osteoblast-specific transcription factor, Runx2: responsiveness to multiple signal transduction pathways, J. Cell. Biochem. 88 (2003) 446–454.

[64] G.S. Stein, J.B. Lian, J.L. Stein, A.J. Van Wijnen, M. Montecino, Transcriptional control of osteoblast growth and differentiation, Physiol. Rev. 76 (1996) 593–629.
[65] J.E. Aubin, Regulation of osteoblast formation and function, Rev. Endocr. Metab. Disord. 2 (2001) 81–94.
[66] P.J. Marie, The molecular genetics of bone formation: implications for therapeutic interventions in bone disorders, Am. J. Pharmacogenomics 1 (2001) 175–187.
[67] R.T. Franceschi, C. Ge, G. Xiao, H. Roca, D. Jiang, Transcriptional regulation of osteoblasts, Ann. N. Y. Acad. Sci. 1116 (2007) 196–207.
[68] L. Wang, M. Singh, L.F. Bonewald, M.S. Detamore, Signalling strategies for osteogenic differentiation of human umbilical cord mesenchymal stromal cells for 3D bone tissue engineering, J. Tissue Eng. Regen. Med. 3 (2009) 398–404.
[69] G.B. Schneider, H. Perinpanayagam, M. Clegg, R. Zaharias, D. Seabold, J. Keller, C. Stanford, Implant surface roughness affects osteoblast gene expression, J. Dent. Res. 82 (2003) 372–376.
[70] A.E. Clark, L.L. Hench, H.A. Paschall, The influence of surface chemistry on implant interface histology: a theoretical basis for implant materials selection, J. Biomed. Mater. Res. 10 (1976) 161–174.
[71] N. Kotobuki, K. Ioku, D. Kawagoe, H. Fujimori, S. Goto, H. Ohgushi, Observation of osteogenic differentiation cascade of living mesenchymal stem cells on transparent hydroxyapatite ceramics, Biomaterials 26 (2005) 779–785.
[72] J.W. Park, H.K. Kim, Y.J. Kim, C.H. An, T. Hanawa, Enhanced osteoconductivity of micro-structured titanium implants (XiVE S CELLplus) by addition of surface calcium chemistry: a histomorphometric study in the rabbit femur, Clin. Oral Implants Res. 20 (2009) 684–690.
[73] A. Ponche, M. Bigerelle, K. Anselme, Relative influence of surface topography and surface chemistry on cell response to bone implant materials. Part 1: physico-chemical effects, Proc. Inst. Mech. Eng. H 224 (2011) 1471–1486.
[74] T. Gross-Aviv, R. Vago, The role of aragonite matrix surface chemistry on the chondrogenic differentiation of mesenchymal stem cells, Biomaterials 30 (2009) 770–779.
[75] S. Scaglione, A. Braccini, D. Wendt, C. Jaquiery, F. Beltrame, R. Quarto, I. Martin, Engineering of osteoinductive grafts by isolation and expansion of ovine bone marrow stromal cells directly on 3D ceramic scaffolds, Biotechnol. Bioeng. 93 (2006) 181–187.